AWARD NUMBER: W81XWH-21-1-0290

TITLE: Smart Coating with Biomimetic Antimicrobial Nanostructures and Strain-Mapping Electronics for Osseointegrated Prostheses to Address Infection and Mechanical Failure Risks

PRINCIPAL INVESTIGATOR: Qing Cao

CONTRACTING ORGANIZATION: University of Illinois at Urbana Champaign
Urbana, IL

REPORT DATE: August 2023

TYPE OF REPORT: Annual

PREPARED FOR: U.S. Army Medical Research and Development Command
Fort Detrick, Maryland 21702-5012

REPORT DOCUMENTATION PAGE

Form Approved
OMB No. 0704-0188

1. REPORT DATE	2. REPORT TYPE	3. DATES COVERED
August 2023	Annual	15Jul2022-14Jul2023

4. TITLE AND SUBTITLE
Smart Coating with Biomimetic Antimicrobial Nanostructures and Strain-Mapping Electronics for Osseointegrated Prostheses to Address Infection and Mechanical Failure Risks

5a. CONTRACT NUMBER

5b. GRANT NUMBER
W81XWH-21-1-0290

5c. PROGRAM ELEMENT NUMBER

6. AUTHOR(S)

Qing Cao

E-Mail: qingcao2@illinois.edu

5d. PROJECT NUMBER

5e. TASK NUMBER

5f. WORK UNIT NUMBER

7. PERFORMING ORGANIZATION NAME(S) AND ADDRESS(ES)

University of Illinois Urbana Champaign, Urbana, IL 61801

8. PERFORMING ORGANIZATION REPORT NUMBER

9. SPONSORING / MONITORING AGENCY NAME(S) AND ADDRESS(ES)

U.S. Army Medical Research and Development Command
Fort Detrick, Maryland 21702-5012

10. SPONSOR/MONITOR'S ACRONYM(S)

11. SPONSOR/MONITOR'S REPORT NUMBER(S)

12. DISTRIBUTION / AVAILABILITY STATEMENT

Approved for Public Release; Distribution Unlimited

13. SUPPLEMENTARY NOTES

14. ABSTRACT

The objective is to develop a smart polymer-foil coating that can be conformally applied on the surface of the skin-penetrating abutment of the osseointegrated prosthetic implants, which simultaneously provides antimicrobial and structural-health-monitoring functionalities. The biomimetic antimicrobial nanopillar arrays on its outer surface prevent surface biofilm formation and reduce risk of superficial infection. Meanwhile, a multiplexed strain sensor arrays on its inner surface intended for conformal contact with the implant offer high sensitivity and high spatial resolution mapping of the strain distribution on the implant, providing active feedbacks to prevent implant mechanical failures. In this year, we have developed a unique process to fabricate flexible multiplexing field-effect transistors and strain sensors with high (~50) gauge factors to precisely detect physiologically relevant implant strain down to 0.01%, based on transfer-printed high-quality single-crystalline silicon nanomembranes. A 3 by 3 multiplexing array has been fabricated. Its strain-mapping performance and functionality has been authenticated through comparison against commercial gauges and finite-element simulations.

15. SUBJECT TERMS
Flexible electronics, sensors, transistors, biomechanics

16. SECURITY CLASSIFICATION OF:			17. LIMITATION OF ABSTRACT	18. NUMBER OF PAGES	19a. NAME OF RESPONSIBLE PERSON
a. REPORT	b. ABSTRACT	c. THIS PAGE			USAMRDC
Unclassified	Unclassified	Unclassified	Unclassified	21	19b. TELEPHONE NUMBER *(include area code)*

TABLE OF CONTENTS

1. Introduction

Bone-anchored limb prostheses, which allow for the direct transfer of external load from the prosthesis to the skeleton without the vulnerable soft-tissue envelope as the intermediate, eliminate complications associated with the socket-stump interface and offer multiple clinical benefits, including improved range of motion, walking ability, sitting comfort, enhanced prosthetic use, and heightened perception of pressure, load, position, and balance. Despite these advantages, current osseointegrated prosthetic limbs are plagued by high infection rate, especially at the implant-skin interface. In addition, the mechanical integrity of the implant system and bone must be preserved under constant stresses induced by the prosthesis and body movement. This research project aims to address the critical issues of preventing infections and monitoring the structural health of percutaneous osseointegrated prosthetic limbs by developing a smart coating in the form of a flexible polymer foil that can be easily wrapped around the cylindrical surface of the skin-penetrating implant exiting the human body. The outer surface of the smart-coating foil features arrays of high-density nanopillars that can kill attached bacterial pathogens through a purely physical process by mimicking the surface topology of cicada wings. It provides an effective, non-toxic antimicrobial barrier to infection at the implant-skin interface. On the inner surface of the smart-coating intended for conformal contact with the implant, it bears a multiplexed array of piezoresistive strain sensors built on transfer-printed flexible, single-crystalline silicon nanomembranes, offering not only high sensitivity with silicon's large piezoresistive coefficient, but also high-spatial-resolution strain-mapping functionality with active selector transistors integrated together. It allows active monitoring of strains experienced by the implant to prevent mechanical failures. The scope of the research includes (1) the development of the process to fabricate the biomimetic antimicrobial nanopillar arrays on flexible polymer substrate and the optimization of the design of their geometries to achieve optimum bactericidal efficacy against common superficial-infection pathogens without human-cell toxicity, (2) the development of multiplexed silicon piezoresistive sensor arrays on flexible polymer substrates for strain mapping over the surface of implants, and (3) verification of the functionalities both in vitro and in vivo in animal models. In year 1 of the project, we have already developed and optimized the antimicrobial nanopillar array designs and verified their antimicrobial activities, structural stability, biocompatibility with human cells, and process scalability. The target of the second year is then to develop the process to prepare multiplexed Si piezoresistive sensor arrays on the other side of the polymer foil and verify their sensitivity and strain-mapping functionality.

2. Keywords

Flexible electronics, sensors, transistors, biomechanics

3. Accomplishments

3.1 What were the major goals of the project?

As listed in the approved SOW, the major goal of this research project in the second year is to complete the second specific aim: Develop multiplexed silicon piezoresistive sensor arrays on flexible polymer substrates for strain mapping over the entire surface of percutaneous abutment. The technological milestones are

1) Optimized design and process to fabricate flexible strain gauges capable of measuring the small strain experienced by implants.
2) Optimized design and process to fabricate flexible selector transistors for multiplexing.
3) Completed sensor array prototype with the strain mapping functionality verified in vitro.

All milestones have been successfully accomplished. And we are moving toward verifying the performance of our dual functional smart-coating foils for osseointegrated orthopedic implants in animal models in the third specific aim, which is scheduled to be completed by the end of the third year.

3.2 What was accomplished under these goals?

3.2.1. Major activities:

The major activities during the second year of the project include (1) the development of the process to transfer-print ultrathin single-crystalline silicon nanomembranes from silicon-on-insulator wafers to plastic substrates; (2) the development of the process to realize high-performance strain sensors in the form of both piezoresistors and Wheatstone bridges based on transferred silicon nanomembranes; (3) the development of the process to fabricate high-performance selector transistors based on transferred silicon nanomembranes; (4) realization of an intergraded strain sensor array composed of 36 piezoresistors and 36 multiplexing transistors; and (5) the authentication of its strain mapping functionality in vitro.

3.2.2. Specific objectives:

The specific objectives are to optimize the designs of the piezoresistive strain sensors and selector transistors built on doped single-crystalline silicon nanomembranes, and then integrate them together to realize multiplexed arrays with performance and functionality verified in vitro. Both objectives have been successfully accomplished.

3.2.3. Significant results:

1. Transfer printing of ultrathin single crystalline silicon nanomembranes.

To monitor strains on percutaneous implants, the ideal sensors need to be highly sensitive, can be multiplexed addressed to achieve high spatial resolution over large area, and can be conformally applied over the curved implant surfaces without modifying the existing implant designs. These requirements can be satisfied by building the strain sensors, together with the active multiplexing electronics, based on single-crystalline silicon nanomembranes transferred onto flexible plastic substrates. The rationale is that silicon membranes will lose their rigidity but instead exhibit excellent flexibility and hence conformability by reducing their thickness below 100 nm, with their excellent electrical properties preserved. We successfully developed a process to form the silicon nanomembranes and subsequently transfer them to plastic substrates as illustrated in Figure 1A. We started from a silicon-on-insulator wafer (SOI, Soitec, 100 nm top layer Si on 1 μm buried oxide). Photolithography defines the photoresist layer on top into a mesh composed of 2D arrays of 10×10 μm^2 square openings with 50 μm pitch. The silicon in the exposed square-opening areas was removed by etching in an inductively coupled plasma (ICP) reactive ion etching (RIE) system (Oxford, The BCl_3 flowing at 10 s.c.c.m., together with Ar flowing at 5 s.c.c.m. maintained a chamber pressure of 10 mTorr. The applied ICP power and RIE power were 300 W and 100 W, respectively. The etching time was 1 min), following the undercut etching of the buried oxide in concentrated HF to release the silicon nanomembrane from the SOI wafer. A layer of polyvinyl alcohol (PVA, Sigma-Aldrich ,15 wt.%) was further spin-casted (2,000 r.p.m. for 2 min) on top to provide both mechanical support and surface protection. A thermal-release tape (Revalpha) was applied onto the PVA film. Peeling off the thermal-release tape picked up the PVA film together with the silicon nanomembrane. The whole film stack was then laminated onto the flat side of the polyimide foil covered with a layer of UV-cured polyurethane (Norland NEA 121, spin-casted at 3,000 r.p.m. for 60 s and then exposed to UV lamp at intensity of 20–25 $mW \cdot cm^{-2}$ for 90 s) as the adhesion layer to bond with the silicon nanomembrane. Heating the foil on hotplate at 160 ^oC released the tape, leaving the silicon nanomembrane with the PVA protection layer on the polyimide receiving substrate. The PVA film was finally removed by immersing the foil in 60 ^oC water bath for 10 min, which completed the silicon nanomembrane transfer-printing process. Image of the silicon mesh transferred on a polyimide foil is shown in Figure 1B.

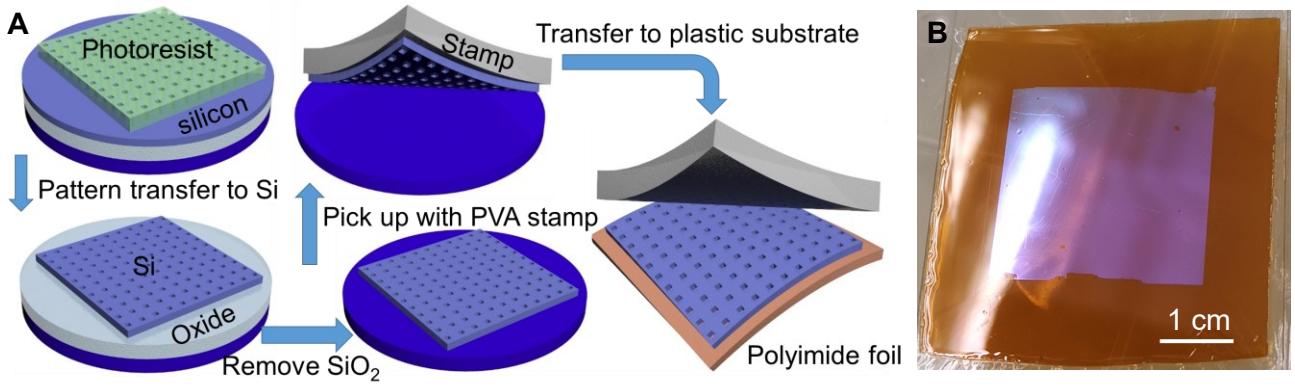

Fig. 1. Transfer printing of single-crystalline Si nanomembranes. (**A**) Process schematics. (**B**) Optical image of a silicon membrane transferred on Kapton.

2. High-performance strain sensors built on silicon nanomembranes on plastic substrates.

Single-crystalline silicon has high piezoresistive coefficient. The applied strain modulates the silicon lattice and thus the material electronic structure, which affects the carrier transport mobility. A critical parameter here is the doping level of silicon. Lower doping concentration leads to higher piezoresistive coefficient, while higher doping level is required to improve the metal-semiconductor contacts and minimize the silicon temperature coefficient of resistance. The doping level of the silicon nanomembrane was precisely controlled via a diffusion doping process prior to transfer. Here a film of phosphorus-containing spin-on-dopant (Filmtronics P509) was blanketly deposited by spin-casting at 3,000 r.p.m. for 30 sec, followed by a soft bake at 110 ^{o}C for 3 min. Annealing at 750-850 ^{o}C for 10 minutes in a three-zone tube furnace (Lindberg) with N_2 (2 L·min^{-1}) and O_2 (1 L·min^{-1}) flow drove the phosphorus to diffuse from the spin-on-dopant into the underlying silicon to achieve a doping level from 1×10^{18} cm^{-3} to 1×10^{20} cm^{-3}, depending on the processing temperature. The doped silicon nanomembranes were then transferred to plastic substrates and then further patterned into simple stain-gauge geometry using standard photolithography followed by RIE of unmasked area in SF_6 plasma. Cr/Au was then defined as the contact electrodes. The optical image of a single-crystalline silicon piezoresistor made on a polyimide foil is displayed in Figure 2A, which contains a silicon strip with the dimension of 20 μm width and 200 μm length. Figure 2B plots its responses under uniaxial tensile strains applied through bonding the substrate on tubes with different radii. The optimum doping level was determined as 1×10^{18} cm^{-3}, which is the minimum required to form a ohmic contact. The gauge factor up to 50 was determined from the slope, much higher than what is possible for metal-foil strain gauges.

To further improve the sensitivity of strain measurement, four silicon piezoresistors were connected in the form of a Wheatstone bridge (Fig. 2C). Since the Wheatstone bridge utilizes difference measurement, its sensitivity is greatly improved compared to simple piezoresistors. Strain down to 0.01% can be reliably measured under a low operation voltage of 1 V, suitable for biomedical applications (Fig. 2D).

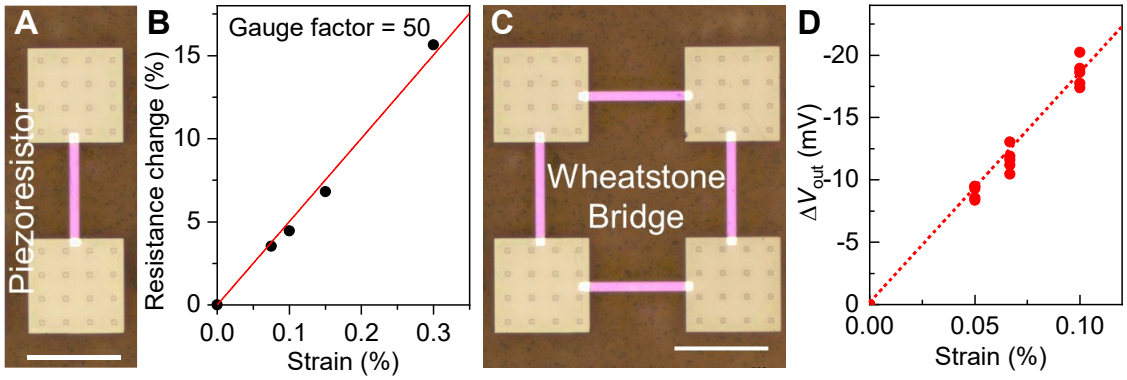

Fig. 2. Flexible strain sensors built on transferred single-crystalline silicon nanomembrane. (**A**) Micrograph of the piezoresistive strain sensor. (**B**) Relative change in resistance of a silicon-nanomembrane piezoresistor as a function of the applied longitudinal tensile strain, with the slope corresponding to a gauge factor of 50. (**C**) Micrograph of the Wheatstone-bridge strain sensor. (**D**) Voltage output (ΔV_{out}) from multiple Wheatstone-bridge strain gauges under tensile strain. The applied bias was 1 V. Scale bars: 200 μm.

3. Field-effect transistors built on transfer-printed silicon nanomembranes on plastic substrates.

To map the strain distribution, it is required to form an array of strain sensors addressed by multiplexing transistors. We have developed the process to fabricate selector transistors also based on transfer-printed silicon nanomembranes on plastics. Here we first selectively n-dope the source/drain regions of the device on the silicon-on-insulator wafer prior to transfer using the diffusion doping process. More specifically, 400 nm SiO_2 was first grown on a silicon-on-insulator wafer by plasma-enhanced chemical vapor deposition (Oxford PECVD system, the deposition was completed in 4.5 min under 20 W and a chamber temperature of 380 °C, using SiH_4 flowing at 8.5 s.c.c.m. and N_2O flowing at 710 s.c.c.m. as the precursors as well as N_2 flowing at 162 s.c.c.m. as the carrier gas to maintain a chamber pressure of 1,000 mTorr). Photolithography was then performed to define patterns of the heavily doped source-drain regions of the selector transistors into the photoresist (AZ-5214), followed by removing the PECVD SiO_2 in the exposed areas using buffered oxide etchant with the photoresist as the etching mask. After stripping the photoresist

in acetone, the spin-on-dopant was applied (Filmtronics P509) and annealed at 850 °C to dope the exposed silicon and thus form the heavily *n*-doped contact regions of transistors. After cooling down to room temperature, the wafer was immersed in HF to remove both the spin-on-dopant and the thermal oxide mask, followed by piranha cleaning to remove the residual phosphorus oxide. After transferring the silicon nanomembrane to the Kapton substrate, the channel regions of each selector transistor were first protected by photoresist defined by photolithography, with the silicon in the exposed regions removed by XeF_2 (Xactix XeF_2 etcher, 3 Torr for 1 min) with high etching selectivity against the polymer substrate, for device isolation. Afterwards, the source-drain electrodes of the selector transistors were patterned into the photoresist by photolithography, followed by electron-beam evaporation of 2 nm Cr/100 nm Au/0.2 nm Cr and lift-off in acetone. The 0.2 nm Cr was used as the seeding layer for the subsequent growth of the gate oxide on top, which was composed of 40 nm HfO_2/30 nm Al_2O_3 bilayer, by atomic layer deposition (ALD, Savannah 100) at 120 °C using Tetrakis(dimethylamido)-hafnium and triethyl-aluminum as precursors, respectively, together with water. The low deposition temperature prevented cracking of the oxide layer resulting from the mismatch of the thermal expansion coefficients, and the top Al_2O_3 layer helped to seal pinholes for higher device yield. 2 nm Cr/100 nm Au was then blanketly deposited by sputtering (AJA). The gate pattern for the selector transistors were defined with one additional photolithography step and the etch-back scheme, using commercial wet etchants (Transene) to remove gold and chromium in exposed areas. These completed flexible transistors exhibited excellent performance (Fig. 3). The device can be operated within a low voltage range of ±3 V, and the extracted effective mobility is above 400 cm^2/Vs.

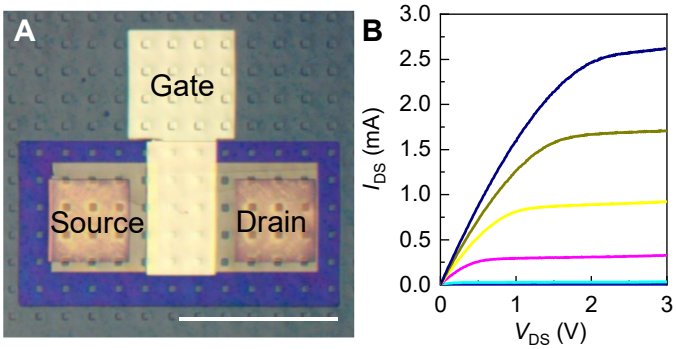

Fig. 3. Multiplexing silicon nanomembrane transistors on plastic substrate. (A) Micrograph of the completed transistor. (**B**) Current-voltage characteristics of the selector transistor (channel width is 200 μm and channel length is 15 μm). The applied gate voltage decreases from 3 V to 0 V with a step of 0.5 V from top to bottom.

4. Multiplexed strain mapping arrays.

The fabricated selector transistors can then be integrated together with Whitestone-bridge strain sensors to yield a distributed network with multiplexed readout for strain mapping over the expansive surfaces of implants (Fig. 4A). In each pixel, the outputs of the piezoresistive bridge are routed first to the four selector transistors corresponding to the columns and rows of the active matrix, and then to the pads (V_+ and V_-) for voltage sensing (Fig. 4B and 4C). Therefore, the pixel output will contribute to the measured voltage difference only with both the row and column selector transistors turned on by positive gate voltage (Fig. 4D). Multiplexing the transistor column/row gate lines and gathering the voltage bias between V_+ and V_- sequentially create a spatial mapping of the strain distribution. The adoption of the fast-switching single-crystalline silicon field-effect transistors as selectors enables high refreshing rate and their large on/off ratio ensures low-crosstalk among sensing elements for better accuracy.

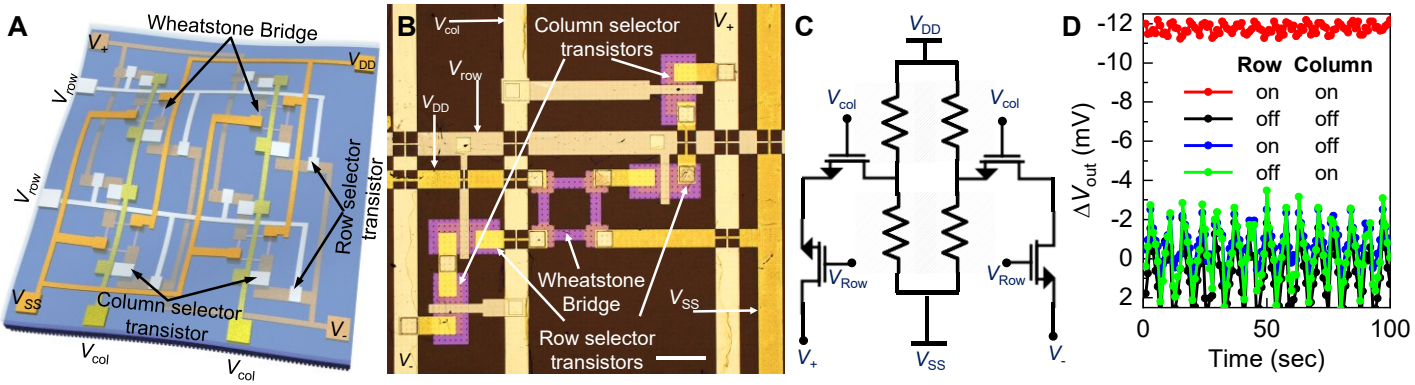

Fig. 4. Multiplexed strain-sensing array. (**A**) Schematic of the multiplexed strain-sensing array. V_{DD}: Supply voltage; V_{SS}: Ground voltage; V_+: Plus-node output-sensing voltage; V_-: Negative-node output-sensing voltage; V_{col}: Column-selection voltage; V_{row}: Row-selection voltage. (**B-C**) Image (part **B**, scale bar: 100 μm) and circuit diagram (part **C**) of a single strain-sensing pixel. (**D**) Output voltage difference (ΔV_{out}) of a pixel under applied tensile strain of 0.05%, measured with different bias conditions of the selector transistors. Applied V_{DD}=1 V.

After completing the multiplexed sensor arrays, an encapsulation layer, which was composed of five repeating stacks of parylene/Al_2O_3/HfO_2/Al_2O_3, was deposited on top. The parylene was deposited using the SCS parylene coater. The deposition chamber was held at room temperature with chamber pressure of 35 mTorr. The temperature of the vaporizer and the pyrolysis furnace was kept at 175 °C and 690 °C, respectively. The film thickness was controlled to about 200 nm by loading 0.5 gram of diparaxylylene

(Galentis) as precursor. The HfO_2 and Al_2O_3 were both deposited at 120 ºC using the ALD process. This encapsulation layer isolated electronics from physiological fluids and successfully protected the devices in accelerated reliability test (> 30 days in phosphate buffered saline (PBS) buffer at 80 °C corresponding to mean time to failure of years, Fig. 5). Both HfO_2 and Al_2O_3 are biocompatible and have good long-term stability in physiological conditions. There might be some Hf and Al ions released through hydrolysis from the deposited thin films. The Al ions released from such nanometer-thick alumina films will be negligible compared to the background Al ion concentration throughout the human body, while the released trace amount of Hf ions is very unlikely to cause any adversary effect, considering their low toxicity.

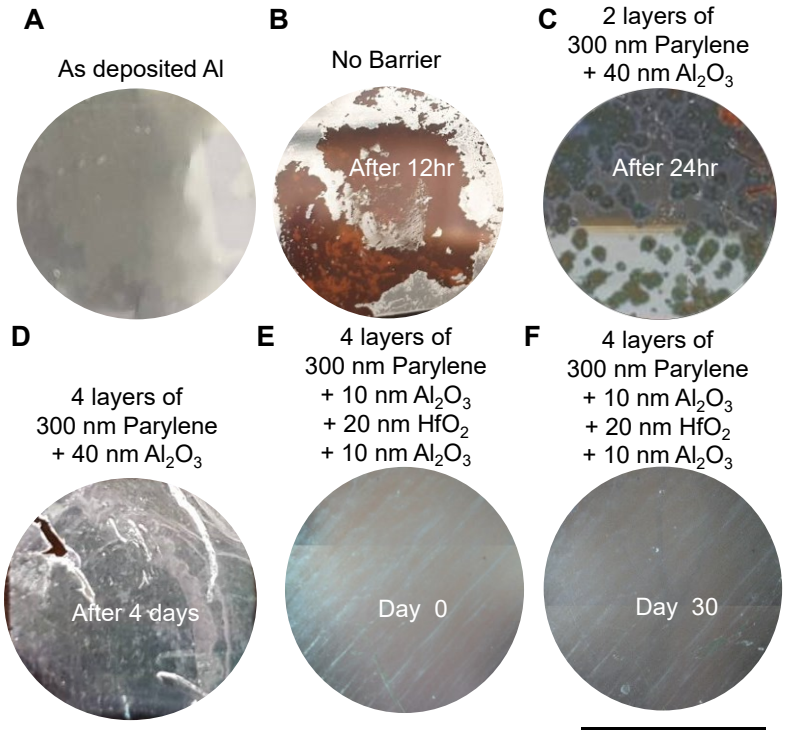

Fig. 5. **Biofluid barrier protecting electronics.** (**A**) Optical image of a uniform layer of aluminum deposited on a Kapton foil as a convenient test vehicle to examine the barrier properties. (**B**) Defects in the aluminum film created by the reaction $2Al+6H_2O \rightarrow 2Al(OH)_3+3H_2$ after continuous immersion in hot PBS for 12 hours without passivation. (**C-D**) Optical images of the aluminum films passivated with two (part **C**) and four (part **D**) layers of parylene/Al_2O_3 stacks after immersion in hot PBS for one and four days, respectively. (**E-F**) Defect-free aluminum film passivated with four layers of the parylene/Al_2O_3/HfO_2/Al_2O_3 stacks before (part **E**) and after (part **F**) immersion in hot PBS for 30 days. Visible defects start to emerge afterwards. Scale bar: 5 mm.

5. In vitro authentication of the performance and functionality of strain mapping arrays integrated on the inner side of the smart-coating foil for osseointegrated implants.

Fig. 6A shows an optical image of a smart-coating foil containing a 3×3 multiplexed sensor array composed of 36 selector transistors and 36 piezoresistors, which was conformally coated around a titanium rod mimicking the skin-penetrating abutment of osseointegrated implants, subject to strain applied using a four-point-bending fixature. Compared to a passive matrix that needs at least 20 input/output lines to connect to 18 high-resolution analog-to-digital converters (ADCs) in the data logger, the active-matrix multiplexing of Wheatstone-bridge strain sensors drastically reduced the total number of interconnect lines by half and the number of required ADCs to two for more efficient implementation of the whole system for strain mapping, although the incorporation of selector transistors increased the fabrication complexity. A thin layer of spin-casted thermally curable polyurethane (Norland NEA121) together with a double-sided, medical adhesive tape (3M 1513) tightly bonded the foil to the implant and mediated the strain transfer. The pixels were located around the circumference and along the axis of the rod, with 4 mm and 8 mm pitch along the transvers and the longitudinal directions, respectively. The differences in local strains were accurately captured by this multiplexed array without off-chip amplification (Fig. 6B). The load-strain curves measured by all nine pixels verified that the strain, which increased linearly with the increase of the applied load, was uniform along the axis of the rod but varied from compressive to tensile from the top to bottom of the rod under four-point bending (Fig. 6C). Readings from five consecutive loading-unloading cycles showed good reproducibility without hysteresis (Fig. 6D).

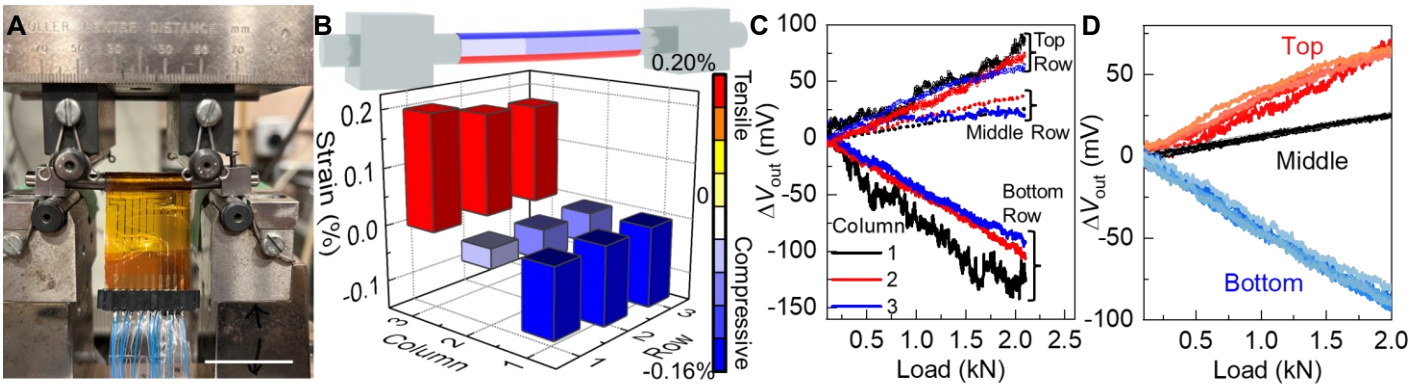

Fig. 6. Multiplexed strain-sensing array to detect strain distribution on a percutaneous abutment of osseointegrated prosthetic implants under four-point bending test. (**A**) Optical image of a rod coated with the smart-coating foil under four-point-bending test. Scale bar: 50 mm. (**B**) Strain distribution along

the rod under 2 kN load as recorded by a 3×3 sensor array. (**C**) ΔV_{out} recorded by each pixel inside the 3×3 array with increasing load applied. Applied V_{DD}=5 V. (**D**) ΔV_{out} recorded by the three strain-sensing pixels in the central column during five consecutive loading cycles.

As shown in Fig. 6A, for this rod mimicking the percutaneous abutment of an osseointegrated prosthetic implant subject to a four-point-bending test, its diameter (d) was 5.5 mm. It was attached to two 9 mm-wide steel cubes with screws to limit the rotation of the rod during measurement, which were placed on two supports that were 60 mm apart (L_{total}). The cylindrical actuators (diameter 10 mm) applied two equal point loads up to 2 kN in total on the rod. The distance (L) between the support and the actuator on the same side was 9.5 mm. With the symmetric geometry of the test step, the fore (F) applied at each contact was 1 kN. The maximum deflection recorded in the center of the rod (δ) was ~0.5 mm.

Based on the classical Euler–Bernoulli beam theory, the maximum stress on the rod (σ) can then be calculated as:

$$\sigma = My/I$$

where M is the moment applied at the middle of the rod defined as:

$$M = F \cdot L,$$

I is the moment of inertia, which can be calculated as

$$I = \frac{\pi\left(d/2\right)^4}{4},$$

and y is the distance from the neutral plane of the rod to its utmost fibre, which is the rod radius (d/2).

Meanwhile, the effective modulus (E) can be calculated as

$$E = \frac{FL(3L_{Total}^2 - 4L^2)}{24\delta I}.$$

The maximum flexural strain is then derived as

$$\varepsilon_{\max} = \frac{\sigma}{E} = \frac{\frac{My}{I}}{\frac{FL(3L_{Total}^2 - 4L^2)}{24\delta I}} = \frac{24\delta y}{(3L_{Total}^2 - 4L^2)} = 0.32\%$$

More accurate results were further obtained based on the finite-element simulation utilizing the software package COMSOL. The 3D geometry in the model comprised the Ti rod, the steel support

blocks, and the cylindrical actuators. The simulated ε_{max} as a function of the load applied is displayed in Fig. 7A, suggesting ε_{max}=0.25% under 2 kN load, which has a better agreement with the 0.21% maximum tensile strain we measured in experiment. The simulated cross-sectional and lateral strain tensor distributions (Fig. 7B and 7C) quantitatively agree with the experimental strain-mapping results shown in Fig. 6B. These results authenticated the accuracy of the strain measured by our flexible sensor arrays.

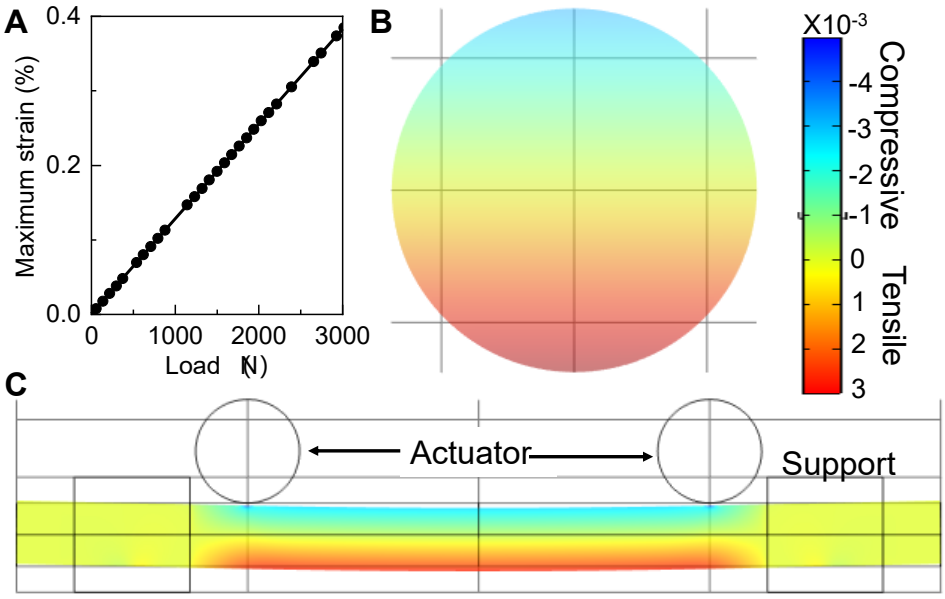

Fig. 7. Finite-element simulation of strain on a rod in four-point-bending test. (**A**) Simulated maximum tensile strain as a function of the force load applied. (**B**) Simulated cross-sectional strain tensor distribution at the middle position along the rod under 2 kN load applied. (**C**) Side view of the simulated deformation of the rod and the corresponding strain tensor distribution.

To further validate the results obtained from the multiplexed single-crystalline silicon piezoresistive sensor arrays and demonstrate their superior performance, we performed the identical four-point bending of the rod with the commercial metal-foil strain gauge (MMF403994, Micro-Measurements) applied on its surface instead (Fig. 8A), as bonded with the same medical-grade polyester tape (3M 1513). The sensor was consisted of a small-section Constantan-alloy filament deposited on a backing plastic substrate. Under applied tensile or compressive strain, the metal wire changes its shape and thus the electrical resistance end-to-end, with a gauge factor of 2. The resistance of the sensor was 120 Ω. During the measurement, it was connected with another three off-chip resistors to form a Wheatstone bridge and the differential voltage signal was amplified with an off-chip amplifier by 1,000×. Since there was no

multiplexing capability with the individually packaged commercial sensor, it was sequentially applied to three different locations around the circumference of the rod, as illustrated in Fig. 8B, to record the strain in three separate load cycles, where the load was increased linearly from 0.1 to 2.1 kN with a rate of 20 $N \cdot s^{-1}$. Even after the 1,000× off-chip amplification of the signal and utilizing a much higher drive voltage of 13 V, the data measured using the conventional metal-foil gauge still exhibited much worse signal-to-noise ratio and thus unreliable measurement results compared to what was recorded using the multiplexed single-crystalline silicon piezoresistive sensor arrays, which have ~25 times higher piezoresistive gauge factor and built-in multiplexing for strain mapping, even though the strain measured under the maximum 2 kN load was quantitatively comparable (Fig. 8C).

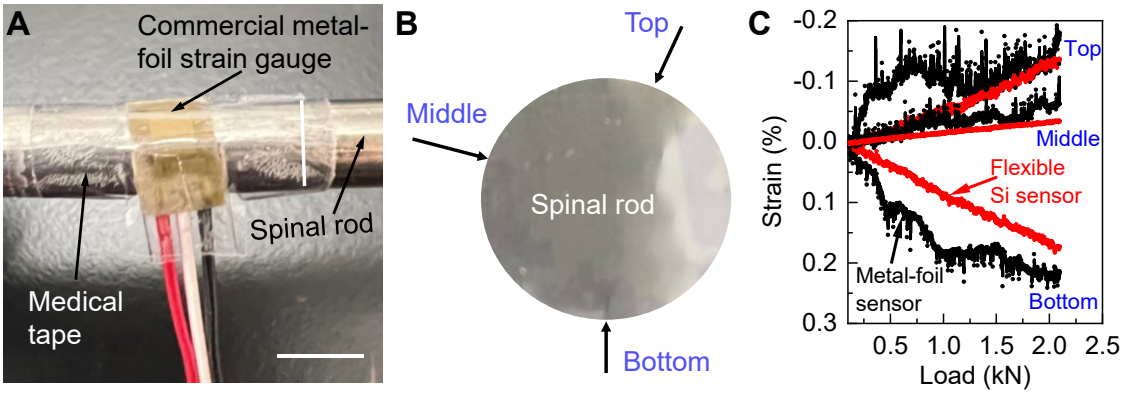

Fig. 8. Benchmark the measurements performed using the commercial metal-foil strain gauges and the flexible silicon piezoresistive sensor arrays. (**A**) Optical image showing a commercial metal-foil sensor applied on the surface of a metal rod. Scale bar: 5 mm. (**B**) Schematic showing the three different locations where the metal-foil gauge was applied, corresponding with the positions of the top, middle, and bottom rows of the flexible silicon strain sensors in their multiplexed array. (**C**) Comparison of the local strain as a function of the load applied, as measured by the commercial metal-foil strain gauges (black) and the flexible single-crystalline silicon piezoresistive sensor array (red).

3.3 What opportunities for training and professional development has the project provided?

This project provided scientific and engineering training to two graduate students involved and the results will become important components in their thesis. Specifically, they received training on the microfabrication, device engineering, electrical characterization, and mechanical engineering.

3.4 How were the results disseminated to communities of interest?

The results have been published as a research article: Yi Zhang et al., “A smart coating with integrated physical antimicrobial and strain-mapping functionalities for orthopedic implants”, Sci. Adv. 9, eadg7397(2023). DOI:10.1126/sciadv.adg7397, which has been featured in many public media. Some examples are listed below:

Materials Today: Antibacterial coatings take the strain on orthopedic implants.

Science Magazine: Smart surgical implant coatings provide early failure warning while preventing infection.

Scienceblog: Smart Coatings Inspired by Bugs Zap Bacteria and Monitor Strain.

ASM International: Bug inspired coating could make for better bone and joint implants.

AZoM: "Smart" Polymer Foil Coating for Orthopedic Implants

Times of India: Smart surgical implant coatings provide early failure warning while stopping infection

3.5 What do you plan to do during the next reporting period to accomplish the goals?

The major goal for the next year is to authenticate the performance and the functionality of the dual-functional smart coatings for osseointegrated prosthetic implants in relevant animal models. The planned study will be carried out in strict accordance with the recommendations in the Guide for the Care and Use of Laboratory Animals of the National Institutes of Health, and by the US Army Medical Research and Materiel Command (USAMRMC) Animal Care and Use Review Office (ACURO). We have identified the appropriate animal models and submitted a protocol that cover the proposed experiments, which has already been approved by the Illinois Institutional Animal Care and Use Committee (IACUC).

4. Impact

4.1 What was the impact on the development of the principal discipline(s) of the project?

Osseointegrated prostheses, despite their different designs, always include a skin-penetrating abutment that connects the prosthesis to the skeletal bone of the residual limb. It is the mechanically weakest part of the osseointegrated prosthetic system by design. The fracture or bending of the abutment, caused by the high, unpredictable, and constant stresses during human-body movements, occurred in 30-40% of patients. It is especially a problem during the patient rehabilitation: on one hand, the bond tissue around the implant needs controlled loading regimes by exercise to stimulate bone mineralization and strength; on the other hand, such exercise must be carefully graded to avoid catastrophic mechanical failures such as bone/implant fracture and implant loosing. Currently, pain assessment using the visual analog scale is utilized in clinical practice as the diagnostic and educational instrument for grading training and avoiding overloads, as the mechanical quality of the osseointegration cannot be determined through conventional medical imaging techniques such as X-ray radiography. Due to lack of quantitative assessment to trigger transitions in care, the overall rehabilitation process is conservatively designed to take at least 12 months and could be as long as 18 months for patients with poor skeletal conditions. In this project, we developed a smart coating for the skin-penetrating abutment. On its inner surface intended for conformal contact with the implant, we incorporated a multiplexed array of piezoresistive strain sensors built on transfer-printed flexible single-crystalline silicon nanomembranes, offering not only high sensitivity with single-crystalline silicon's large piezoresistive coefficient, but also high-spatial-resolution strain-mapping functionality, with silicon active selector transistors integrated together. We have demonstrated that the fabricated flexible sensor arrays can precisely measure the strain down to 0.01% as typically experienced by osseointegrated implants. They offer much higher signal to noise ratio and spatial resolution compared to what is possible with conventional strain gauges based on either metal foils or rigid semiconductors, without modifying the internal structure of the implant. It can provide active feedback during the rehabilitation process and especially early warning regarding the instrument failures to improve patient outcomes. It will also help us to better understand the biomechanics regarding the osseointegration and the bone-tissue system.

4.2 What was the impact on other disciplines?

The developed ultrasensitive flexible strain-mapping arrays can be used in other biomedical applications such as monitoring the pressure distribution along the catheters.

4.3 What was the impact on technology transfer?

A patent application has been filed. We will work with the office of technology management at the University of Illinois to push for the commercialization of this technology, through either licensing to industry partners or in a startup company.

4.4 What was the impact on society beyond science and technology?

Nothing to Report.

5. Changes/Problems

5.1 Changes in approach and reasons for change

Nothing to Report.

5.2 Actual or anticipated problems or delays and actions or plans to resolve them

Nothing to Report.

5.3 Changes that had a significant impact on expenditures

Nothing to Report.

5.4 Significant changes in use or care of human subjects, vertebrate animals, biohazards, and/or select agents

Nothing to Report.

5.5 Significant changes in use or care of human subjects

Nothing to Report.

5.6 Significant changes in use or care of vertebrate animals.

Nothing to Report.

5.7 Significant changes in use of biohazards and/or select agents

Nothing to Report.

6. Products

Publications, conference papers, and presentations

Yi Zhang, Jinsong Cui, Kuan-Yu Chen, Shanny H. Kuo, Jaishree Sharma, Rimsha Bhatta, Zheng Liu, Austin Ellis-Mohr, Fufei An, Jiahui Li, Qian Chen, Kari D. Foss, Hua Wang, Yumeng Li, Annette M. McCoy, Gee W. Lau, and Qing Cao*, “A Smart Coating with Integrated Physical-Antimicrobial and Strain-Mapping Functionalities for Orthopedic Implants,” Science Advances. 9, eadg7393 (2023).

Inventions, patent applications, and/or licenses

A non-provisional patent entitled “Nanostructured Bactericidal Polymer Foil” was filed on 08/30/2021. The inventors are Qing Cao and Yi Zhang, and the U.S. Patent Application No. is 17/460,561.

7. Participants & Other Collaborating Organizations

7.1 What individuals have worked on the project?

Name:	*Qing Cao*
Project Role:	*PI*
Researcher Identifier (e.g. ORCID ID):	*0000-0002-5844-2376*
Nearest person month worked:	*1*
Contribution to Project:	*Prof. Cao is responsible for the overall coordination, intellectual inputs, experimental design, data analysis, and supervision of all aspects of this project.*

Name:	*Annette McCoy*
Project Role:	*Co-I*
Nearest person month worked:	*1*
Contribution to Project:	*Prof. McCoy developed animal models and prepared the IACUC and ACURO protocols.*

Name:	*Yi Zhang*
Project Role:	*Graduate Student*
Nearest person month worked:	*12*
Contribution to Project:	*Mr. Zhang fabricated the strain-sensor arrays and tested their performances.*
Funding Support:	*PPG-MRL Ph.D. Fellowship*

Name:	*Jinsong Cui*
Project Role:	*Graduate Student*
Nearest person month worked:	6
Contribution to Project:	*Mr. Cui helped with the device fabrication.*

7.2 Has there been a change in the active other support of the PD/PI(s) or senior/key personnel since the last reporting period?

Nothing to Report.

7.3 What other organizations were involved as partners?

Nothing to Report.

8. Special Reporting Requirements

Not Applicable.

9. Appendices

Copy of journal article.